# A Historical Perspective and A Review of the Fundamental Principles in Modeling 3D Periodic Structures with an Emphasis on volumetric EBGs

M. Kafesaki[1], and C. M. Soukoulis[1,2]
[1] *Institute of Electronic Structure and Laser (IESL), Foundation for Research and Technology Hellas (FORTH), P.O. Box 1527, 71110 Heraklion, Crete, Greece, and Department of Materials Science and Technology, University of Crete, Greece.*
*and*
[2] *Ames Laboratory-USDOE and Department of Physics and Astronomy, Iowa State University, Ames, IA 50011, USA*

## 8.1. INTRODUCTION

### A. Electromagnetic (Photonic) Band Gap materials or Photonic Crystals

Electromagnetic band gap (EBG) materials (known as photonic crystals (PCs) or photonic band gap (PBG) materials) are a novel class of artificially fabricated structures which have the ability to control and manipulate the propagation of electromagnetic waves [1-3]. Properly designed photonic crystals can prohibit the propagation of light, or allow it along only certain directions, or localize light in specified areas. They can be constructed in one, two, and three dimensions (1D, 2D, and 3D), with either dielectric or/and metallic materials.

The ability of PCs to control the propagation of light has its origin in their photonic band structure. The concept of photonic band structure [4-5] arises in analogy to the concept of electronic band structure. Just as electron waves, traveling in the periodic potential of a crystal, are arranged into energy bands separated by band gaps, we expect the analogous phenomenon to occur when electromagnetic (EM) waves propagate in a medium in which the dielectric constant varies periodically in space. Photonic band gap materials or photonic crystals are the structures which show such a phenomenon, i.e., produce a forbidden frequency gap in which all propagating states are prohibited. The investigation of these materials is a topic of intensive studies by many groups, both theoretically and experimentally [1-3].

The photonic band gap property of photonic crystals makes them the electromagnetic analog of the electronic semiconductor crystals, although in the electromagnetic case the periodicity alone does not guarantee the existence of a full photonic band gap. Nonetheless, a great advantage of the PCs is that although in semiconductors the periodicity is predetermined, the periodicity in the PCs can be changed at will, thus changing the frequency range of the photonic band gap. Such structures have been built in the microwave and recently in the far-infrared regime, and their potential applications continue to be examined. However, the greatest scientific challenge in the field of PCs is to fabricate composite structures possessing spectral gaps at frequencies up to the optical region.

The first prescription for a periodic dielectric structure [6] that possesses a full photonic band gap rather than a pseudogap was given by Ho, Chan and Soukoulis at Iowa State University (ISU). This proposed structure was a periodic arrangement of dielectric spheres in a diamond-like lattice. It was found that photonic band gaps exist over a wide region of filling ratios; for both dielectric spheres in air and air spheres in a dielectric; and for refractive-index contracts between spheres and host as low as 2. However, this diamond dielectric structure is not easy to fabricate, especially in the micron and submicron length scales, for infrared or optical devices. In the same time frame as ISU's findings about the diamond structure [6], Yablonovitch was devising [7] an ingenious way of constructing a structure with the symmetry of the diamond lattice. This was achieved by properly drilling cylindrical holes through a dielectric block. Such a structure with only three sets of holes (three-cylinder structure) became the first experimental structure [7] that demonstrated the existence of a (full or complete) photonic band gap, in agreement with the predictions [8] of the theoretical calculations. This is a successful example where the theory was used to design dielectric structures with desired properties. It is very interesting to note that after fifteen years since the introduction [6] of the diamond lattice by the ISU group, it still possesses [9] the largest photonic band gap.

Another example of a successful synergy between theory and experiment is encountered in the layer-by-layer structure (see Fig. 1), the so-called "wood pile" structure. The layer-by-layer structure was designed by the Iowa State group [10] and has a full three-dimensional photonic band gap over a wide range of structural parameters. The structure consists of layers of rods, with a stacking sequence that repeats every fourth layer. It was first fabricated [11] by stacking alumina cylinders, and it was demonstrated to have a full three-dimensional photonic band gap at 12-14 GHz.

Another interesting class of photonic crystals is the A7 class of structures [12]. These structures have rhombohedral symmetry and can be generated by connecting lattice points of the A7 structure by cylinders. The A7 class of structures can be described by two structural parameters that can be varied to optimize the gap. For special values of the parameters the structure reduces to simple cubic, diamond, and the Yablonovitch 3-cylinder structure. Gaps as large as 50 % are found [12] in the A7 class of structures for well optimized values of the structural parameters; fabrication of these structures would be a very interesting task.

The fabrication and the testing of PC structures is a task that has attracted intensive efforts, dating back to the original efforts by Yablonovitch [15]. Fabrication can be either easy or extremely difficult, depending upon the desired wavelength of the band gap and the level of dimensionality. Since the wavelength of the band gap scales directly with the lattice constant of the photonic crystal, lower frequency structures that require larger dimensions are easier to fabricate. At the other extreme, optical wavelength PBGs require PC lattice constants less than one micron. Building PCs in the optical regime is a major challenge in PBG research and requires methods that push the current state-of-the-art micro- and nano-fabrication techniques. Clearly, the most challenging PBG structures are fully 3D structures with band gaps in the infrared or optical regions of the spectrum. This area of PBG research has been one of the most active, and perhaps most frustrating, in recent years.

The first attempts towards PBG structures operating in the infrared or optical regime have targeted the miniaturization of the existing microwave PBG structures. Since 1991, both Yablonovitch and Scherer have been working towards reducing the size of Yablonovitch's [7] 3-cylinder structure to micrometer length scales [16]. However, it is very difficult to drill uniform holes of appreciable depth with micron diameters. Thus, Scherer's efforts were only partially successful in producing a photonic crystal with a gap at optical frequencies. Another approach for the miniaturization of Yablonovitch's 3-cylinder structure was undertaken by a group at the Institute of Microtechnology in Mainz, Germany, in collaboration with FORTH, in Greece, and the Iowa State University, using deep x-ray lithography (LIGA) [17]. In this method PMMA resist layers with thickness of 500 microns were irradiated to form a "three-cylinder" structure. Since the dielectric constant of the PMMA is not large enough for the formation of a PBG, the holes in the PMMA structure were filled with a ceramic material. After the evaporation of the solvent, the samples were heat treated; and a lattice of ceramic rods corresponding to the holes in the PMMA structure remained. A few layers of this structure were fabricated; it was measured to have a band gap centered at 2.5 THz. A SEM view of this structure, with a lattice constant of 114$\mu$m, is shown In Fig. 2. Recent experiments are currently trying to fill the PMMA holes with a metal.

Attempts at the miniaturization of the layer-by-layer wood pile structure shown in Fig. 1 include a miniature version that was fabricated [18] by laser rapid prototyping using a laser-induced direct-write deposition from the gas phase. The structure consisted of oxide rods that were sub-micron in size; the measured photonic band gap was centered at 2 THz. Recent work, at Sandia National Laboratory by Lin [19], and at Kyoto University by Noda [20], has demonstrated growth up to five layers of the layer-by-layer wood pile structure, at both the 10 micron and 1.5 micron wavelengths. The measured transmittance of these structures showed a band gap centered at 30 THz and 200 THz, respectively. These are really spectacular achievements. They were able to overcome very difficult technological challenges, in planarization, orientation, and 3D growth at the required micrometer length scales.

Another approach to obtain PCs in submicron regimes is by using colloidal suspensions. Colloidal suspensions have the ability to spontaneously form bulk 3D crystals with lattice parameters on the order of 1-10 nm. Also, 3D dielectric lattices have been developed from a solution of artificially grown monodisperse spherical $SiO_2$ particles. However, both these procedures give structures with a quite small dielectric contrast ratio (less than 2), which is not enough to achieve a full band gap. A lot of effort is going into finding new methods for increasing the dielectric contrast ratio in these structures. Several groups [21-28] are trying to produce ordered macroporous materials of titania, silica, and zirconia by using the emulsion droplets as templates, around which material is deposited through a sol-gel process. Subsequent drying and heat treatment have yielded solid materials with spherical pores left behind the emulsion droplets. Another very promising technique in fabricating photonic crystals at optical wavelengths is 3D holographic lithography [29]. Very recently, high-quality large-scale wood pile structures, operating at 1.5 micron, have been fabricated by direct laser writing [30].

Since the fabrication of 3D photonic crystals at optical wavelengths is still a difficult process, an alternative method has been proposed. A three-layered dielectric structure is created in the vertical direction, with the central layer having a higher dielectric constant than the upper and lower dielectric layers. In such a structure light is confined in the vertical direction by traditional waveguiding due to dielectric index mismatch, and in the lateral direction by the presence of a two-dimensional (2D) photonic crystal. There are two routes that have been followed, one where the upper and lower dielectric layers are air and the other where the upper and lower dielectric layers have dielectric constants smaller than the central layer but much higher than one. The first structure is called a self-supported membrane [31], while the second is referred as a regular waveguide [32]. It is not yet resolved which structure has lower losses [31-35]. It is clear however that for optoelectronic applications the membrane-based photonic crystals might not be easy to use. It is therefore of considerable importance to find out what type of structure has the lowest

losses and the best efficiency of bends.

One of the most challenging applications of the miniature photonic-crystals is in the telecommunication regime, for the construction of fully photonic integrated circuits (PICs). Essential building blocks for the realization of photonic crystal based PICs are PC waveguides, waveguide-bends, and combiners, that are constructed by properly forming defects in the PCs. Light then is confined in the defects' path and is guided along this one-dimensional channel, the photonic crystal waveguide, because the three-dimensional PC prevents it from escaping into the bulk crystal. Simulations have predicted very exciting results that would have significant impact on applications; but the inclusion of defects in an already difficult to build 3D PC further complicates the fabrication requirements.

### B. Left-handed Materials or Negative Index Materials

Recently, there have been many studies about metamaterials that have a negative refractive index, $n$. These materials, called left-handed materials (LHMs), theoretically discussed first by Veselago [36], have simultaneously negative electrical permittivity, $\epsilon$, and magnetic permeability, $\mu$. A practical realization of such metamaterials, employing split ring resonators (SRRs) and continuous wires (see Fig. 3), was first introduced by Pendry [37, 38], who suggested that a slab of metamaterial with $n = -1$ could act as a perfect lens. [39].

The first realization of some of Pendry's ideas was achieved by Smith et. al. in 2000 [40], and since then various new samples (with the same composition of SRRs and wires) have been prepared [41, 42], all of which have been shown to exhibit a pass band in which it was assumed that $\epsilon$ and $\mu$ are both negative. This assumption was based on measuring independently the transmission, $T$, of the wires alone, and then the $T$ of the SRRs alone. If the peak in the combined metamaterial composed of SRRs+wires was in the stop bands for the SRRs alone (which is thought to correspond to negative $\mu$) and for the wires alone (which is thought to correspond to negative $\epsilon$) the peak was considered to be left-handed (LH). Further support to this interpretation was provided by the demonstration that some of these materials exhibit negative refraction of electromagnetic waves [43].

Subsequent experiments [44] have reaffirmed the property of negative refraction, giving strong support to the interpretation that these metamaterials can be correctly described by negative permeability, due to the SRRs, and negative permittivity, due to the wires. However, as was shown in Ref. [45], this is not always the case since the SRRs, in addition to their magnetic response, which was first described by Pendry [38], exhibit also a resonant electric response in frequencies not far from the magnetic response frequency. The electric response of the SRRs, which is demonstrated by closing their air gaps (destroying their resonant magnetic response), is identical to that of cut-wires and it is added to the electric response ($\epsilon$) of the wires. Consequently, the effective plasma frequency, $\omega_p'$, of the combined system of wires and SRRs (or closed SRRs) is always lower than the plasma frequency of only the wires, $\omega_p$. With this consideration and the analytical expressions for $\epsilon$ and $\mu$ which stem from it [45], one is able to explain and reproduce all of the low frequency transmission, $T$, and reflection, $R$, characteristics of the SRRs+wires based LHMs.

Moreover, considering the electric response of the SRRs and combining it with the fact that closing of the SRR gaps leaves this response unchanged, an easy criterion [45] to identify if an experimental transmission peak is LH or right-handed (RH) is readily obtained: If closing the gaps of the SRRs in a given LHM structure removes from the $T$ spectrum the peak close to the position of the SRR dip, this is strong evidence that the $T$ peak is indeed left-handed. If the gap above the peak is removed, the peak is most likely right-handed. This criterion is very valuable in experimental studies, where one can not easily obtain the effective $\epsilon$ and $\mu$. The criterion is used experimentally and is found that some $T$ peaks that were thought to be LH, turned out to be right-handed [46].

There has also been a significant amount of numerical work [47–52] in which the complex transmission and reflection amplitudes for a finite length of metamaterial were calculated. Using these data a retrieval procedure was applied to obtain the effective permittivity $\epsilon$ and permeability $\mu$, under the assumption that the metamaterial can be treated as homogeneous. This procedure confirmed [53, 54] that a medium composed of SRRs and wires could indeed be characterized by effective $\epsilon$ and $\mu$ with negative real parts over a finite frequency band, and thus a refractive index also having a negative real part.

Recently, efforts have been made to fabricate LH structures at the THz frequency range. A magnetic response has been observed from SRRs at 2 THz [55], 6 THz [56] and 100 THz [57]. This response was experimentally observed through the electric excitation of the magnetic resonance (EEMR) [58], i.e., the excitation of the magnetic resonance through the external electric field. This EEMR effect occurs for given orientations of the gaps of the SRR with respect to the external electric field, independently of the propagation direction, and makes possible the experimental characterization of small artificial magnetic structures [58], as it eliminates the necessity of in-plane incidence of an external EM field.

## 8.2. THEORETICAL AND NUMERICAL METHODS

To study theoretically and numerically the propagation of EM waves in PCs and LH materials, a variety of theoretical and numerical methods have been employed. These methods are used to calculate either the *band structure* of such materials (considering them as infinite) or the *transmission properties* of finite PC or LH slabs.

The most widely used methods, which can be applied to both PCs and LH materials, are the plane wave (PW) method, the transfer matrix method (TMM), and the finite difference time domain (FDTD) method. In the following we will describe these methods and we will present their capabilities and their main disadvantages.

The starting point in all these methods is Maxwell's equations in isotropic materials:

$$\nabla \cdot \mathbf{D} = 0, \qquad \nabla \cdot \mathbf{H} = 0, \tag{8.1}$$

$$\nabla \times \mathbf{E} = -\frac{\partial \mathbf{B}}{\partial t}, \qquad \nabla \times \mathbf{H} = \frac{\partial \mathbf{D}}{\partial t}, \tag{8.2}$$

where

$$\mathbf{D}(\mathbf{r}) = \epsilon_0 \epsilon(\mathbf{r}) \mathbf{E}(\mathbf{r}), \qquad \mathbf{B}(\mathbf{r}) = \mu_0 \mu(\mathbf{r}) \mathbf{H}(\mathbf{r}). \tag{8.3}$$

### A. Plane Wave Method

The plane wave method [59, 60] is mainly used to calculate the dispersion relation, hence, the band structure of perfect photonic crystals, considering them as infinite systems, or of photonic crystals with isolated defects, in combination with a supercell scheme [2]. It is usually applied to lossless, dielectric, non-magnetic media. The dispersion relation is calculated by transforming the problem into an eigenvalue problem, which gives the eigenfrequencies $\omega(\mathbf{k})$ for each wave vector $\mathbf{k}$.

Since the media under study are characterized by a spatially varying dielectric function, $\epsilon(\mathbf{r})$, Maxwell's equations (8.2), considering a harmonic time dependence of the form $e^{+j\omega t}$ and $\mu = 1$, are recast to their time-harmonic form

$$\nabla \times \mathbf{E} = -j\omega\mu_0 \, \mathbf{H}, \qquad \nabla \times \mathbf{H} = j\omega\epsilon(\mathbf{r})\epsilon_0 \, \mathbf{E}. \tag{8.4}$$

The two Eqs. (8.4) can be combined to generate equations containing only the magnetic or only the electric field:

$$\nabla \times (\epsilon^{-1}(\mathbf{r}) \nabla \times \mathbf{H}) = \frac{\omega^2}{c_0^2} \mathbf{H} \tag{8.5}$$

and

$$\nabla \times (\nabla \times \mathbf{E}) = \frac{\omega^2}{c_0^2} \epsilon(\mathbf{r}) \mathbf{E}, \tag{8.6}$$

with $c_0^2 = 1/\mu_0\epsilon_0$. The eigenfrequencies $\omega$ are obtained by the solution of either Eq. (8.5) or Eq. (8.6). Here we will proceed using Eq. (8.5).

At this point, we have to note that the vector nature of the wave equations (8.5) and (8.6) is of crucial importance. Early attempts [2] adopting the scalar wave approximation led to qualitatively wrong results, as unphysical longitudinal modes appeared in the solutions.

In the simplest and most common case, where $\epsilon(\mathbf{r})$ is a real and frequency independent periodic function of $\mathbf{r}$, the solution of the problem scales with the spatial period of $\epsilon(\mathbf{r})$: for example, reducing the size of the structure by a factor of two will not change the spectrum of electromagnetic modes other than scaling all frequencies up by a factor of two.

Because of the periodicity of the problem, we can translate the periodic function $\epsilon^{-1}(\mathbf{r})$ of (8.5) into the reciprocal space, writing it as a sum of plane waves with their wave vectors being given by the reciprocal lattice vectors, $\mathbf{G}$, i.e.,

$$\epsilon^{-1}(\mathbf{r}) = \sum_{\mathbf{G}} \epsilon^{-1}(\mathbf{G}) \exp(-j\mathbf{G} \cdot \mathbf{r}). \tag{8.7}$$

Moreover, we can make use of Bloch's theorem to expand the magnetic field of (8.5) in terms of Bloch waves:

$$\mathbf{H}(\mathbf{r}) = \sum_{\mathbf{K}} \mathbf{H}_{\mathbf{K}} \exp(-j \, \mathbf{K} \cdot \mathbf{r}), \tag{8.8}$$

where $\mathbf{K} = \mathbf{k} + \mathbf{G}$, $\mathbf{k}$ is a vector in the first Brillouin zone (BZ), $\mathbf{H}_\mathbf{K}$ are the Fourier components of the periodic amplitude of the $\mathbf{k}$ Bloch's wave, and the summation is taken in fact over the vectors $\mathbf{G}$.

The substitution of Eqs. (8.7) and (8.8) into Eq. (8.5) leads to the eigenvalue problem

$$\sum_{\mathbf{K}'} \epsilon^{-1}_{\mathbf{K},\mathbf{K}'} \mathbf{K} \times (\mathbf{K}' \times \mathbf{H}_{\mathbf{K}'}) = -\frac{\omega^2}{c_0^2} \mathbf{H}_\mathbf{K}, \tag{8.9}$$

where $\epsilon^{-1}_{\mathbf{K},\mathbf{K}'} = \epsilon^{-1}(\mathbf{K} - \mathbf{K}') = \epsilon^{-1}(\mathbf{G} - \mathbf{G}')$ (see (8.7)).

At this point we have to note that dielectric functions with sharp spatial discontinuities require an infinite number of plane waves in their Fourier expansion; this can not be achieved in realistic calculations where the sums have to be truncated. To avoid this problem, we smear out the interfaces of the dielectric objects in the unit cell. For example, for modeling a cylinder of radius $a$ with a dielectric function $\epsilon$, we employ the smeared dielectric function

$$\epsilon(\mathbf{r}) = 1 + (\epsilon - 1)/(1 + \exp((r - a)/w), \tag{8.10}$$

where the width $w$ of the interface is chosen as a small fraction of the radius $a$ ($\approx 0.01a$-$0.05a$). In practice, we incorporate the smearing and define the dielectric function $\epsilon(\mathbf{r})$ over a grid in real space; then we compute its transform in our finite plane wave basis set to obtain $\epsilon(\mathbf{G} - \mathbf{G}')$; and the term $\epsilon^{-1}(\mathbf{G} - \mathbf{G}')$ of (8.9) is then obtained by the inversion of the $\epsilon(\mathbf{G} - \mathbf{G}')$ matrix. This procedure yields much better convergence than the alternative method of determining $\epsilon^{-1}(\mathbf{r})$ in real space and then performing a Fourier transform to obtain $\epsilon^{-1}(\mathbf{G} - \mathbf{G}')$.

The transversality of the $\mathbf{H}$ field implies that $\mathbf{K} \cdot \mathbf{H}_\mathbf{K} = 0$; thus, $\mathbf{H}_\mathbf{K}$ can be written as

$$\mathbf{H}_\mathbf{K} = h_{\mathbf{K},1} \mathbf{e}_1 + h_{\mathbf{K},2} \mathbf{e}_2, \tag{8.11}$$

where the unit vectors $\mathbf{e}_1$ and $\mathbf{e}_2$ form with $\mathbf{K}$ an orthogonal triad $(\mathbf{e}_1, \mathbf{e}_2, \mathbf{K})$. The solution of (8.9) for the magnetic field (8.11) then reduces to the eigenvalue system

$$\sum_{\mathbf{K}'} \mathrm{M}_{\mathbf{K},\mathbf{K}'} h_{\mathbf{K}'} = \frac{\omega^2}{c_0^2} h_\mathbf{K}, \tag{8.12}$$

which gives the allowed frequencies $\omega(\mathbf{k})$. In (8.12)

$$\mathrm{M}_{\mathbf{K},\mathbf{K}'} = \mid \mathbf{K} \mid\mid \mathbf{K}' \mid \epsilon^{-1}_{\mathbf{K},\mathbf{K}'} \begin{pmatrix} \mathbf{e}_2 \cdot \mathbf{e}'_2 & -\mathbf{e}_2 \cdot \mathbf{e}'_1 \\ -\mathbf{e}_1 \cdot \mathbf{e}'_2 & \mathbf{e}_1 \cdot \mathbf{e}'_1 \end{pmatrix}, \quad h_\mathbf{K} = \begin{pmatrix} h_{\mathbf{K},1} \\ h_{\mathbf{K},2} \end{pmatrix}, \quad h_{\mathbf{K}'} = \begin{pmatrix} h_{\mathbf{K}',1} \\ h_{\mathbf{K}',2} \end{pmatrix}, \tag{8.13}$$

and the unit vectors $\mathbf{e}'_1$ and $\mathbf{e}'_2$ form an orthogonal triad with $\mathbf{K}'$.

As was mentioned earlier, in the above eigenfrequencies calculation we used the wave equation for the magnetic field, Eq. (8.5), and not Eq. (8.6) for the electric field. In principle, we also could follow the same procedure for Eq. (8.6). However, the resulting eigenvalue problem would then be either an eigenvalue problem with a non-hermitian matrix, M, or a generalized (instead of a simple) eigenvalue problem, which requires, in both cases, a more demanding computational procedure for its solution than the one associated with Eq. (8.12). Consequently, it is advantageous to use Eq. (8.5) rather than Eq. (8.6) to obtain the band structure of a PC.

In practice, the photonic band structure given by the frequencies $\omega(\mathbf{k})$ is computed over several sets of high symmetry points in the Brillouin zone, or on a grid in the Brillouin zone if the density of states is needed. A plane wave convergence check is an essential step in that computation.

The first structure [2] considered by researchers with the plane wave approach was a fcc structure composed of low index dielectric spheres in a high index dielectric ($\epsilon$) background. There is no full band gap (i.e., gap for all directions in the BZ and thus for all directions of propagation of the EM waves) between the second and third bands, while a sizable complete gap exists between the eighth and ninth bands (8-9 gap). The 8-9 position of the gap is a generic feature of the band structure of fcc photonic band gap materials that is worth mentioning. The size (gap width over midgap frequency) of the full band gap is about 8% for a refractive index contrast of 3.1.

A structure that has been investigated thoroughly, as was mentioned in the introduction, is the diamond structure [3,6,8,9]. The diamond structure presents a full three-dimensional photonic band gap between the second and third bands (2-3 gap), for a wide range of filling ratios. This gap exists for (i) high dielectric spheres on the sites of the diamond lattice, (ii) low dielectric spheres on the diamond sites, and (iii) the diamond structure connected by dielectric rods. The best performing gap (29%) is reached for the diamond structure with 89% air spheres, i.e., a multiply connected sparse structure. A similar large gap (30%) is also found for the diamond structure connected with

dielectric rods with about a 30% dielectric filling fraction. These gap magnitudes have been obtained for a refractive index contrast of 3.6, appropriate for a GaAs background and air spheres.

The band structure and the corresponding density of states (DOS) for a diamond lattice is shown in Fig. 4, for a system of dielectric spheres of $n = 3.6$ and a filling ratio 0.34. This filling ratio corresponds to the diamond close packing, where the 2-3 full band gap stops to exist. The system shown in Fig. 4 was first studied by Ho, Chan and Soukoulis [6] by the PW method. It was soon realized [2, 13] that for a 0.34 filling ratio with such high index spheres, the PW method is very difficult to converge. The same conclusion was reached by Moroz [61]. When one is using the PW method, one has to exercise extreme care when handling dielectric spheres having a high index of refraction, i.e., one needs a lot of terms in the Fourier transform to obtain accurate results. Even today's PW methods, especially the MIT photonic bands (MPB) package [62], still need an extrapolation to infinitely many plane waves to yield convergent results. Band structure calculations of photonic crystals with high index dielectric spheres might give better convergent results if the multiple scattering (or photonic-KKR) method [61] was used.

### B. Transfer Matrix Method (TMM)

While the method described in the previous section focuses on a particular wave vector (i.e., gives $\omega = \omega(\mathbf{k})$), there are complementary methods that focus on a single frequency (i.e., give $\mathbf{k} = \mathbf{k}(\omega)$), like the transfer matrix method (TMM). The TMM was first used to calculate the band structure of a PC by Pendry and MacKinnon [63].

The TMM is able to calculate the band structure of PC-based structures, including structures of complex or frequency dependent dielectric functions (like metallic ones). This feature is not readily available through the PW method. The main power of the TMM though is its ability to calculate the stationary scattering properties, i.e., the complex transmission ($t$) and reflection ($r$) amplitudes, of finite slabs of PCs and of LH materials. Such calculations are extremely useful in the interpretation of experimental measurements of the transmission and reflection data.

The calculation of the transmission and reflection coefficients for plane wave scattering from a slab of PC or LH metamaterial is performed by assuming that the slab, which is finite along the direction of the incoming incident wave ($z$ direction here), is placed between two semi-infinite slabs of vacuum, and by employing the time-harmonic Maxwell's equations (8.4). (By imposing periodic boundary conditions, the slab is considered infinite along the directions perpendicular to that of the propagation direction of the incident wave.)

The approach used with the TMM consists of the calculation of the EM field components at a specific $z$ plane (e.g., after the slab) from the field components at a previous $z$ plane (e.g., before the slab). For the implementation of this procedure Eqs. (8.4) are discretized, employing a rectangular grid on which the fields and the material parameters are defined. The result is a system of local difference equations:

$$\begin{aligned}
E_x(i,l,k+1) &= E_x(i,l,k) + jc\omega\mu_0\mu(i,l,k)H_y(i,l,k) + \\
&\frac{jc}{a\omega\epsilon_0\epsilon(i,l,k)}\{a^{-1}[H_y(i-1,l,k) - H_y(i,l,k)] - b^{-1}[H_x(i,l-1,k) - H_x(i,l,k)]\} - \\
&\frac{jc}{a\omega\epsilon_0\epsilon(i+1,l,k)}\{a^{-1}[H_y(i,l,k) - H_y(i+1,l,k)] - \\
&\qquad b^{-1}[H_x(i+1,l-1,k) - H_x(i+1,l,k)]\}, \qquad (8.14)\\
E_y(i,l,k+1) &= E_y(i,l,k) - jc\omega\mu_0\mu(i,l,k)H_x(i,l,k) + \\
&\frac{jc}{b\omega\epsilon_0\epsilon(i,l,k)}\{a^{-1}[H_y(i-1,l,k) - H_y(i,l,k)] - b^{-1}[H_x(i,l-1,k) - H_x(i,l,k)]\} - \\
&\frac{jc}{b\omega\epsilon_0\epsilon(i,l+1,k)}\{a^{-1}[H_y(i-1,l+1,k) - H_y(i,l+1,k)] - \\
&\qquad b^{-1}[H_x(i,l,k) - H_x(i,l+1,k)]\}, \qquad (8.15)\\
H_x(i,l,k+1) &= H_x(i,l,k) - jc\omega\epsilon_0\epsilon(i,l,k+1)E_y(i,l,k+1) + \\
&\frac{jc}{a\omega\mu_0\mu(i-1,l,k+1)}\{a^{-1}[E_y(i,l,k+1) - E_y(i-1,l,k+1)] - \\
&\qquad b^{-1}[E_x(i-1,l+1,k+1) - E_x(i-1,l,k+1)]\} - \\
&\frac{jc}{a\omega\mu_0\mu(i,l,k+1)}\{a^{-1}[E_y(i+1,l,k+1) - E_y(i,l,k+1)] - \\
&\qquad b^{-1}[E_x(i,l+1,k+1) - E_x(i,l,k+1)]\}, \qquad (8.16)\\
H_y(i,l,k+1) &= H_y(i,l,k) + jc\omega\epsilon_0\epsilon(i,l,k+1)E_x(i,l,k+1) +
\end{aligned}$$

$$\frac{jc}{b\omega\mu_0\mu(i,l-1,k+1)}\{a^{-1}[E_y(i+1,l-1,k+1)-E_y(i,l-1,k+1)]- b^{-1}[E_x(i,l,k+1)-E_x(i,l-1,k+1)]\}- \frac{jc}{b\omega\mu_0\mu(i,l,k+1)}\{a^{-1}[E_y(i+1,l,k+1)-E_y(i,l,k+1)]- b^{-1}[E_x(i,l+1,k+1)-E_x(i,l,k+1)]\}. \quad (8.17)$$

In the above equations $\epsilon(i,l,k)$ and $\mu(i,l,k)$ are the relative electrical permittivity and magnetic permeability at the grid cell $(i,l,k)$, and $a,b,c$ are the dimensions of each grid cell along the $x,y,z$ directions, respectively. We have to mention that the components $E_z$, $H_z$ are eliminated from further consideration, due to the transversality of the fields, and that the field components $E_x(i,l,k)$, $E_y(i,l,k)$, $H_x(i,l,k)$, $H_y(i,l,k)$ are defined at different points of their associated grid cell $(i,l,k)$ (they are mutually displaced by a half grid cell). Special attention has to be taken with the material discretization because the symmetries of the structure also have to be maintained in the discretized system.

Equations (8.14)-(8.17) connect the field components at the $k+1$ plane with those at the $k$ plane. After rearrangement of terms they can take the form

$$\begin{pmatrix}\mathbf{E}(k+1)\\ \mathbf{H}(k+1)\end{pmatrix} = \mathrm{T}\begin{pmatrix}\mathbf{E}(k)\\ \mathbf{H}(k)\end{pmatrix}. \quad (8.18)$$

The matrix T is the transfer matrix, which allows one to compute the whole solution from a previously known $z$ slice. In the vacuum the matrix T can be diagonalized exactly; its left and right eigenvectors define the plane wave basis for the scattering problem. By propagating the vacuum basis vectors through the sample and by subsequent decomposition of the results with respect to the vacuum basis again, one obtains the T matrix of the slab. With T known, the scattering amplitudes $r$ and $t$ can be obtained by using the relation between T and the scattering matrix, S, in this basis:

$$\mathrm{T} = \begin{pmatrix} t_+ - r_+t_-^{-1}r_- & r_+t_-^{-1} \\ -t_-^{-1}r_- & t_-^{-1}\end{pmatrix}, \qquad \mathrm{S} = \begin{pmatrix} t_+ & r_+ \\ r_- & t_-\end{pmatrix}. \quad (8.19)$$

(S defines the transmission and reflection amplitudes for waves incident from the left or right of a slab, $t_\mp$ and $r_\pm$.) For economy of computer time and memory, the transfer matrices of the sample slices can be applied consecutively and algorithmically, i.e., not as matrix multiplications. Intermediate renormalization steps account for the exponential growth of some modes inside the sample and keep the simulation stable [48]. Implementations of the TMM can be made to be quite efficient because they rely mainly on linear algebra operations such as matrix factorization and successive inversion.

For the calculation of the band structure, $\mathbf{k}(\omega)$, of a system, one has to compute the eigenvalues of T while also applying periodic boundary conditions along the direction of propagation. Details about this procedure can be found in Ref. [63].

The TMM method has been extensively applied to band structure calculations of PCs containing absorptive and frequency dispersive (e.g., metallic) materials. It has been applied also to the simulation of the scattering properties of finite PCs, of PCs with defects, PCs with complex and frequency dependent dielectric functions [64], and also of left-handed materials composed of SRRs of various shapes and metallic wires [45, 50]. In all these cases the agreement between the theoretical calculations and the experimental results, where available, has been very good.

In Fig. 5 we show an example of the application of the TMM method to the calculation of the transmission coefficient through a slab of a metamaterial composed of rectangular SRRs, printed on a dielectric board, and of closed SRRs [45]. As has been already mentioned, when the gaps of the SRRs are closed, their magnetic response is switched-off while their electric response remains unchanged. This can be seen clearly in Fig. 5; the spectrum of the closed-SRRs is almost identical to that of the SRRs, with the exception of the dip at $\omega a/c \approx 0.04$ (where $\mu < 0$) and the peak at $\omega a/c \approx 0.095$ (where $\mu < 0$, $\epsilon < 0$, i.e., a LH peak; the $\mu < 0$ here is due to the presence of the inner ring, which also exhibits a magnetic response [65]).

### C. Finite Difference Time Domain (FDTD) method

Like the transfer matrix method, the FDTD method can be also used to calculate both band structure and scattering properties of PCs and LH materials, and it also involves discretization of the Maxwell's equations. The difference here is that, while the TMM is employed for steady state solutions, the FDTD method is used for general time dependent solutions. The steady state solutions then are obtained through Fast Fourier transforming the time domain results.

This permits the study of both the transient and the steady state response of a system. An additional advantage is the possibility of obtaining a broad-band steady state response with just a single calculation, as the excitation signal can be a pulse rather than a monochromatic wave.

Since FDTD is a time domain method, the starting point for its implementation is the time dependent Maxwell equations; specifically Eqs. (8.2). The curl equations (8.2) are discretized using a rectangular grid (which stores the field components and the material properties $\epsilon$ and $\mu$) and central differences for the space and the time derivatives. The procedure results in a set of finite difference equations, which updates the field components in time. The equations for the update of $E_x$ and $H_x$ read as follows:

$$E_x^{n+1}(i,l,k) = E_x^n(i,l,k) + \frac{\Delta t}{\epsilon_0 \epsilon(i,l,k)} \quad [\frac{H_z^{n+1/2}(i,l+1/2,k) - H_z^{n+1/2}(i,l-1/2,k)}{b} - \frac{H_y^{n+1/2}(i,l,k+1/2) - H_y^{n+1/2}(i,l,k-1/2)}{c}], \tag{8.20}$$

$$H_x^{n+1/2}(i,l,k) = H_x^{n-1/2}(i,l,k) + \frac{\Delta t}{\mu_0 \mu(i,l,k)} \quad [\frac{E_y^n(i,l,k+1/2) - E_y^n(i,l,k-1/2)}{c} - \frac{E_z^n(i,l+1/2,k) - E_z^n(i,l-1/2,k)}{b}]. \tag{8.21}$$

The corresponding equations for $E_y$, $E_z$, $H_y$, $H_z$ are similar to the above. The FDTD equations for various types of materials, together with computational procedure, source incorporation procedure, stability criteria etc. are presented in a very clear and complete way in Ref. [66]. Here we just review some of the main points of the FDTD calculation procedure as it is applied to PCs and LH materials, to familiarize the reader with the method and to facilitate the comparison with the other methods. In Eqs. (8.20) and (8.21) $E_x^n(i,l,k)$ and $H_x^n(i,l,k)$ are the $x$ components of the electric and magnetic field in the $(i,l,k) \equiv (ia, lb, kc)$ grid cell, at the $n$ time step (where $t = t_n = n\Delta t$), etc.; $a, b, c$ are, respectively, the dimensions of the grid cell along the $x, y, z$ directions, and $\Delta t$ is the time step.

Here, like in the TMM, the different electromagnetic field components are located at different points of their associated grid cell, following the well known Yee's scheme [66]: the **E**-field components, which are calculated at times $n\Delta t$, are located at the face centered points of the grid cell, while the **H**-field components, which are calculated at times $(n+1/2)\Delta t$, are located at the edges of the grid cell (every **E** component is surrounded by four circulating **H** components and vice versa). This scheme results in second order accuracy and a complete fulfillment of all four of Maxwell's equations, although only two equations (Eqs. (8.2)) are directly employed.

Using the FDTD equations (like (8.20), (8.21)), one can obtain $\mathbf{E}(t)$ and $\mathbf{H}(t)$ at any point within a finite slab and, through fast Fourier transforming, $\mathbf{E}(\omega)$ and $\mathbf{H}(\omega)$. The transmission (reflection) coefficient, $T$ ($R$), is then calculated by dividing the Fourier transform of the transmitted (reflected) Poynting vector, $\mathbf{S} = \mathrm{Re}[\mathbf{E}(\omega) \times \mathbf{H}^*(\omega)]/2$, by the incident Poynting vector. Note that what is calculated is the power coefficient, $T = |t|^2$ ($R = |r|^2$), a real quantity, and not the complex transmission (reflection) amplitude.

The transmission calculation procedure usually consists of sending a pulse (e.g., a Gaussian) and then obtaining the transmitted frequency domain fields [83] $\mathbf{E}(\omega)$, $\mathbf{H}(\omega)$, and thus $T$. The slab along the directions perpendicular to the direction of propagation of the incident wave can be considered either as infinite or as finite. The first case is achieved by using periodic boundary conditions at the associated boundaries and the second by using absorbing boundary conditions (i.e., the incident wave at the boundaries is absorbed by them). Absorbing boundary conditions are also used to close the computational cell in the propagation direction. The most efficient absorbing boundary conditions that have been applied to date are the perfectly matched layer (PML) conditions [66], while Liao's conditions [66, 67] are also efficient and widely used.

Equations (8.20), (8.21) and the corresponding ones for the other field components describe dielectric media with no losses. The FDTD study of *dielectric media with losses* ($\epsilon = \epsilon_r - j\epsilon_i$) is achieved usually by introducing a conductivity, $\sigma = \omega\epsilon_0\epsilon_i$, through an external current ($\mathbf{J} = \sigma\mathbf{E}$) added to the first of the equations given in Eqs. (8.2). This leads to a modification of the terms appearing in the standard finite difference equations, but leaves the computational procedure unaltered (see [66]).

To model *dispersive materials*, like metals, as is required, e.g., in the study of metallic PCs or of LH materials, one has to introduce a specific dispersion model (e.g., Drude model, $\epsilon(\omega) = 1 - \omega_p^2/(\omega^2 - j\omega\gamma)$) and translate the equation $\mathbf{D} = \epsilon_0\epsilon(\omega)\mathbf{E}$ (see Eqs. (8.3)) into the time domain [68]. The result is an additional FDTD equation on the top of the standard FDTD equations. (Note that the relation $\mathbf{D} = \epsilon_0\epsilon\mathbf{E}$ does not hold in the time domain when dispersive materials are involved; thus **D** and **E** have to be calculated independently within the FDTD procedure.) A similar procedure is employed also for magnetic materials, $\mu = \mu(\omega)$ [68].

The FDTD method [66, 69] is an excellent tool for the study of the transmission through finite slabs, as it can model almost arbitrary material combinations and microstructure configurations. It has been utilized in many systems,

containing dielectric or metallic components [70–74] as well as in materials with non-linear dielectric properties [75–77]. Methods to transform the output near fields to radiating far-fields have been also employed [66]; this is particularly necessary for antenna problems, where far-field radiation patterns are desired.

The FDTD method, as was mentioned earlier, can be also utilized for band structure calculations [73, 78, 79]. In this case the computational domain is usually a single unit cell of the periodic structure, with periodic boundary conditions in all its boundaries. An excitation containing a wide frequency range is used to excite the allowed modes for each wave vector. These modes appear as spikes in the Fourier transform of the time domain fields.

An example of the application and the potential of the FDTD method is shown in Fig. 6. Figure 6(a) shows the magnetic field (at a specific time point) of a Gaussian (in space) beam, which undergoes reflection and refraction at the interface between air and a hexagonal photonic crystal constructed with dielectric rods in air, at a frequency belonging to the convex photonic band, i.e., the band in which the group velocity in the PC is opposite to the **k** vector [80]. In such a frequency band the PC should behave as a LH system; indeed the refracted beam in Fig. 6(a), which undergoes negative refraction, unambiguously proves the validity of this consideration. Figure 6(b) demonstrates the guiding of an EM wave through a straight PC waveguide, formed by removing one row of holes from an hexagonal 2D photonic crystal.

### 8.3. COMPARISON OF THE DIFFERENT NUMERICAL TECHNIQUES

As we mentioned in the previous section, the PW method is usually used to treat infinite periodic systems, giving their dispersion properties. Although it can be applied only in systems with non-dispersive components (frequency independent $\epsilon$ and $\mu$), the PW method is the fastest and the easiest to apply method. It can give within a single calculation all the spectrum, $\omega$, for a given wave vector. Its main disadvantages are its inability to treat systems with dispersive components and finite media, and its relative difficulty to treat systems with defects. In the last case a supercell scheme has to be employed, which, in many cases, leads to calculations that are very computer time and memory consuming.

The transfer matrix method (TMM) on the other hand is able to calculate the band structure of systems with dispersive components, but it is less easy to apply than the PW method is. It is usually used for the calculation and analysis of the stationary scattering properties of finite-in-length samples. Among the most important advantages of the TMM is its ability to treat samples with almost arbitrary internal structure and arbitrary material combinations (metallic, lossy etc.), giving the complex transmission and reflection amplitudes, i.e., magnitude, phase and polarization information. The simultaneous amplitude and the phase knowledge can be used in the inversion of the transmission and reflection data, to obtain the effective material parameters ($\epsilon$ and $\mu$) for the systems under study (provided that the effective medium approach is valid).

Among the drawbacks of the TMM is the necessity of the discretization of the unit cell, which introduces some numerical artifacts and some constraints into the shape and the size of the components inside the unit cell. For example, to simulate "tiny" components, as is usually required in the study of LH materials, one needs very fine discretization, practically possible only within a non-uniform discretization scheme. Otherwise large calculation times and large memory requirements are unavoidable.

The FDTD method, like the TMM, can also model finite slabs with almost arbitrary internal structure and material combinations. Its main advantages compared to the TMM is that it can give the transmission properties over a wide spectral range with just a single calculation. It also can give time domain pictures of the fields and the currents over the entire computational domain. Moreover, it can treat defects with no additional computational complications.

Concerning the disadvantages of the FDTD method, part of them stem from the inherent discretizations required, and they were discussed above in connection with the TMM. In the case of dispersive materials, though, one encounters additional problems, coming from the time scale that the dispersion model introduces, as the time step of the method ($\Delta t$) can not be much larger than the characteristic time scale of the dispersion model. This constraint imposes restrictions in the frequency regimes that can be studied and, through them, in the size of the structures involved.

Concerning the application of FDTD in band structure calculations, the level of difficulty is similar to that of the TMM. The advantages and disadvantages compared to TMM are essentially those mentioned in the two previous paragraphs, in connection with the calculations of the scattering parameters.

Apart of the three methods that we have described and analyzed in this chapter, there are additional methods that have been applied to the study of PCs and LH materials, although less extensively. Some of those are variations of the PW, TMM and FDTD methods. Among the existing methods, one worth mentioning is the multiple scattering (MS) or photonic-KKR method [61, 81], which is a vectorial extension of the well known electronic band structure calculation method KKR, and its modification known as the layered-MS method [82]. They can both give band structure and transmission properties of PCs and LH materials, treating accurately the dispersive components, defects, as well as

high index contrast systems. Their main disadvantages are the heavy formalism, the difficulties in the computational procedure, and the large calculation times.

### 8.4. CONCLUSIONS

We presented a brief historical review of the theoretical and experimental efforts in designing and fabricating photonic crystals (PCs) and left-handed materials (LHMs), starting from the first successful designs and arriving at the latest developments. The latter included photonic band gaps in the infrared or optical regime and materials with negative magnetic permeability at around 100 THz. We also presented the theoretical and experimental challenges and the problems of the field, as well as its current status, and several of the current research directions.

We also reviewed the three most successful and widely used numerical techniques employed in the studies of PCs and LHMs. These are the plane wave method, the transfer matrix method and the finite difference time domain method. We presented the key ideas and equations of each method, and discussed their capabilities and disadvantages. Finally we presented a few representative results from each method. We are excited about the future applications of PCs and LHMs, and the prospects for using these computational techniques to help design, fabrication, and testing of these PCs and LHMs.

Acknowledgments.
It is a pleasure to thank our colleagues E. N. Economou, P. Markos, T. Koschny, N. Katsarakis, M. Sigalas, E. Ozbay, S. Foteinopoulou, E. Lidorikis, and D. R. Smith for their collaboration and insights. Financial support by the EU projects DALHM, Metamorphose and Phoremost, and by NATO CLG 981471, and DARPA (Contract No. MDA972-01-2-0016) are acknowledged. This work was partially supported by Ames Laboratory (Contract. No. W-7405-Eng-82). Financial support by the Greek Ministry of Education, through PYTHAGORAS project is also acknowledged.

[1] C. M. Soukoulis, Ed., *Photonic Crystals and Light Localization in the 21st Century*, NATO ASI, Series C, vol. 563, 2001.
[2] C. M. Soukoulis, Ed., *Photonic Band Gaps and Localization,* New York: Plenum, 1993; *Photonic Band Gap Materials*, Dordrecht: Kluwer, 1996.
[3] J. D. Joannopoulos, R. D. Mead, and J. N. Winn, *Photonic Crystals*, Princeton University Press, 1995.
[4] E. Yablonovitch, *Phys. Rev. Lett.*, vol. 58, pp. 2059-2062, May 1987.
[5] S. John, *Phys. Rev. Lett.*, vol. 58, pp. 2486-2489, June 1987; S. John, *Physics Today*, vol. 32, pp. 33-38, May 1991.
[6] K. M. Ho, C. T. Chan, and C. M. Soukoulis, *Phys. Rev. Lett.*, vol. 65, pp. 3152-3155, December 1990.
[7] E. Yablonovitch, T. J. Gmitter, and K. M. Leung, *Phys. Rev. Lett.*, vol. 67, pp. 2295-2298, October 1991.
[8] C. T. Chan, K. M. Ho, and C. M. Soukoulis, *Europhys. Lett.*, vol. 16, no. 6, pp. 563-565, 1991.
[9] M. Moldovan and E. L. Thomas, *Nature Materials*, vol. 3, pp. 593-600, September 2004.
[10] K. M. Ho, C. T. Chan, C. M. Soukoulis, R. Biswas, and M. Sigalas, *Solid State Comm.*, vol. 89, pp. 413-416, February 1994.
[11] E. Ozbay, A. Abeyta, G. Tuttle, M. C. Tringides, R. Biswas, M. Sigalas, C. M. Soukoulis, C. T. Chan, and K. M. Ho, *Phys. Rev. B*, vol. 50, pp. 1945-1948, July 1994.
[12] C. T. Chan, S. Datta, K. M. Ho, and C. M. Soukoulis, *Phys. Rev. B*, vol. 49, pp. 1988-1991, July 1994.
[13] H. S. Sozuer, J. W. Haus, and R. Inguva, *Phys. Rev. B*, vol. 45, pp. 13962-13972, June 1992.
[14] T. Suzuki and P. Yu, *J. Opt. Soc. of Am. B*, vol. 12, pp. 570-582, April 1995.
[15] E. Yablonovitch, and T. J. Gmitter, *Phys. Rev. Lett.*, vol. 63, pp. 1950-1953, October 1989.
[16] C. Cheng and A. Scherer, *J. Vac. Sci. Tech. B*, vol. 13, pp. 2696-2700, November-December 1995; C. Cheng et. al. *Physica Scripta*, vol. 68, pp. 17-19, 1996.
[17] G. Feiertag et al. in *Photonic Band Gap Materials* ed. by C. M. Soukoulis, Kluwer, Dordrecht, 1996, pp. 63-69; G. Feiertag et. al., *Appl. Phys. Lett.*, vol. 71, pp. 1441-1443, September 1997.
[18] M. C. Wanke, O. Lehmann, K. Muller, Q. Wen, and M. Stuke, *Science*, vol. 275, pp. 1284-1286, February 1997.
[19] S. Y. Lin et. al., *Nature*, vol. 394, pp. 251-254, July 1998; J. G. Fleming and S. Y. Lin, *Optics Letters*, vol. 24, pp. 49-51, January 1999.
[20] N. Yamamoto, S. Noda and A. Chutinan, *Jpn. J. Appl. Phys.*, vol. 37, pp. L1052-L1054, September 1998; S. Noda et. al., *Appl. Phys. Lett.*, vol. 75, pp. 905-907, August 1999; S. Noda et. al., *Science*, vol. 289, pp. 604-606, July 2000.
[21] J. E. G. J. Wijnhoven and W. L. Vos, *Science*, 281, pp. 802-804, August 1998.
[22] A. Imhof and D. J. Pine, *Nature*, vol. 389, pp. 948-951, October 1997.
[23] B. T. Holland et. al., *Science*, vol. 281, pp. 538-540, July 1998.
[24] A. A. Zakhidov et. al., *Science*, vol. 282, pp. 897-901, October 1998.
[25] G. Subramania et. al., *Appl. Phys. Lett.*, vol. 74, pp. 3933-3935, June 1999; G. Subramarian et. al. *Adv. Mater.* vol. 13, 443-446, March 2001.
[26] Y. Vlasov, X. Z. Bo, J. C. Sturm and D. J. Norris, *Nature*, vol. 414, pp. 289-293, November 2001.
[27] A. Blanco et. al., *Nature*, vol. 405, pp. 437-440, May 2000.
[28] O. D. Velev and E. Kaler, *Adv. Mater.*, vol. 12, pp. 531-534, April 2000, and references therein.
[29] M. Campbell et al., *Nature*, vol. 404, pp. 53-56, March 2000.
[30] M. Deubel et. al. *Nature Materials*, vol. 3, pp. 444-447, July 2004.
[31] O. Painter, J. Vuckovic, and A. Scherer, *J. Opt. Soc. Am. B*, vol. 16, pp. 275-285, February 1999; B. D'Urso et. al. *J. Opt. Soc. Am. B*, vol. 15, pp. 1155-1159, March 1998.
[32] H. Benisty et. al. *J. Light Technol.*, vol. 17, pp. 2063-2077, November 1999.
[33] M. Kafesaki, M. Agio, and C. M. Soukoulis, *J. Opt. Soc. Am. B*, vol. 19, pp. 2232-2240, September 2002; *J. Appl. Phys.*, vol. 96, pp. 4033-4038, October 2004.
[34] W. Bogaerts et. al., *Photonics Tecnnol. Lett.*, vol. 13, pp. 565-567, June 2001.
[35] E. Chow et. al., *Nature*, vol. 407, pp. 983-986, October 2000; E. Chow et. al. *Optics Letters*, vol. 26, pp. 286-288, March 2001.
[36] V. G. Veselago, *Sov. Phys. Usp.*, vol. 10, pp. 509-514, January-February 1968 [*Usp. Fiz. Nauk*, vol. 92, pp. 517, 1967].
[37] J. B. Pendry, A. J. Holden, W. J. Stewart, and I. Youngs, *Phys. Rev. Lett.*, vol. 76, pp. 4773-4776, June 1996; *J. Phys.: Condens. Matt.*, vol. 10, pp. 4785-4809, June 1998.
[38] J. B. Pendry, A. J. Holden, D. J. Robbins, and W. J. Stewart, *IEEE Trans. on Microwave Theory and Techn.*, vol. 47, pp. 2075-2084, November 1999.
[39] J. B. Pendry, *Phys. Rev. Lett.*, vol. 85, pp. 3966-3969, October 2000.
[40] D. R. Smith, W. J. Padilla, D. C. Vier, S. C. Nemat-Nasser, and S. Schultz, *Phys. Rev. Lett.*, vol. 84, pp. 4184-4187, May 2002.
[41] R. A, Shelby, D. R. Smith, S. C. Nemat-Nasser, and S. Schultz, *Appl. Phys. Lett.*, vol. 78, pp. 489-491, January 2001; M. Bayindir, K. Aydin, E. Ozbay, P. Markoš, and C. M. Soukoulis, *Appl. Phys. Lett.*, vol. 81, pp. 120-122, July 2002.
[42] K. Li, S. J. McLean, R. B. Gregor, C. G. Parazzoli, and M. Tanielian, *Appl. Phys. Lett.*, vol. 82, pp. 2535-2537, April 2003.
[43] R. A. Shelby, D. R. Smith, and S. Schultz, *Science*, vol. 292, pp. 77-79, April 2001.
[44] C. G. Parazzoli, R. Gregor, K. Li, B. E. C. Koltenbach, and M. Tanielian, *Phys. Rev. Lett.*, vol. 90, pp. 107401-(1-4), March 2003; A. A. Houck, J. B. Brock, and I. L. Chuang, *Phys. Rev. Lett.*, vol. 90, pp. 137401-(1-4), April 2003.
[45] T. Koschny, M. Kafesaki, E. N. Economou, and C. M. Soukoulis, *Phys. Rev. Lett.*, vol. 93, pp. 107402-(1-4), September

2004.
[46] N. Katsarakis, T. Koschny, M. Kafesaki, E. N. Economou, E. Ozbay, and C. M. Soukoulis, *Phys. Rev. B*, vol. 70, pp. 201101-(1-4), November 2004.
[47] T. Weiland, R. Schummann, R. B. Greegor, C. G. Parazzoli, A. M. Vetter, D. R. Smith, D. V. Vier, and S. Schultz, *J. Appl. Phys.*, vol. 90, pp. 5419-5424, 2001; P. Markoš and C. M. Soukoulis, *Phys. Rev. E*, vol. 65, pp. 036622-(1-8), March 2002.
[48] P. Markoš, and C. M. Soukoulis, *Phys. Rev. E*, vol. 66, pp. 045601-(1-4), October 2002; *Phys. Rev. B*, vol. 65, pp. 033401-(1-4), January 2002.
[49] J. Pacheco, T. M. Grzegorczyk, B.-I. Wu, Y. Zhang, and J. A. Kong, *Phys. Rev. Lett.*, vol. 89, pp. 257401-(1-4), December 2002.
[50] P. Markoš and C. M. Soukoulis, *Optics Express*, vol. 11, pp. 649-661, April 2003; P. Markos and C. M. Soukoulis, *Optics Letters*, vol. 28, pp. 846-848, May 2003.
[51] S. O'Brien and J. B. Pendry, *J. Phys.: Condens. Matter*, vol. 14, pp. 4035-4044, April 2002; *ibid*, vol.14, pp. 6383-6394, July 2002.
[52] S. O'Brien, et. al., *Phys. Rev. B*, vol. 69, pp. 241101-(1-4), June 2004.
[53] D. R. Smith, S. Schultz, P. Markoš, and C. M. Soukoulis, *Phys. Rev. B*, vol. 65, pp. 195104-(1-5), April 2002.
[54] T. Koschny, P. Markoš, D. R. Smith, and C. M. Soukoulis, *Phys. Rev. E*, vol. 68, pp. 065602-(1-4), December 2003.
[55] T. J. Yen et. al. *Science*, vol. 303, pp. 1494-1496, March 2004.
[56] N. Katsarakis et. al., *Optics Letters* (to appear in 2005).
[57] S. Linden et. al., *Science*, vol. 306, pp. 1351-1353, November 2004.
[58] N. Katsarakis, T. Koschny, M. Kafesaki, E. N. Economou, and C. M. Soukoulis, *Appl. Phys. Lett.*, vol. 84, pp. 2943-2945, April 2004.
[59] K. Sakoda, *Optical properties of photonic crystals*, Berlin: Springer, 2001.
[60] P. R. Villeneuve and M. Piche, *Progr. Quantum Electron.*, vol. 18, iss. 2, pp. 153-200, 1994.
[61] A. Moroz, *Phys. Rev. B*, vol. 66, pp. 115109-(1-15), September 2002.
[62] The MIT Photonic Bands (MPB) package can be found at http:// ab-initio.mit.edu/mpb/
[63] J. B. Pendry and A. MacKinnon, *Phys. Rev. Lett.*, vol. 69, pp. 2772-2775, November 1992; J. B. Pendry, *J. Mod. Opt.*, vol. 41, pp. 209-229, February 1994.
[64] M. M. Sigalas, C. T. Chan, K. M. Ho, and C. M. Soukoulis, *Phys. Rev. B*, vol. 52, pp. 11744-11751, October 1995; D. R. Smith, S. Shultz, N. Kroll, M. M. Sigalas, K. M. Ho, and C. M. Soukoulis, *Appl. Phys. Lett.*, vol. 65, pp. 645-647, August 1994.
[65] M. Kafesaki, Th. Koschny, R. S. Penciu, T. F. Gundogdu, E. N. Economou, and C. M. Soukoulis, *J. of Opt. A: Pure Appl. Opt.*, vol. 7, pp. S12-S22, January 2005.
[66] A. Taflove and S. C. Hagness, *Computational Electrodynamics: The Finite Difference Time Domain Method*, Boston: Artech House, 2000.
[67] Liao boundary conditions are based on extrapolation of the fields in space and time by use of a Newton backward-difference polynomial. They are introduced in Z. P. Liao, H. L. Wong, B. P. Yang, and Y. F. Yuan, *Sci. Sin., Ser. A*, vol. 27, pp. 1063-1076, 1984. Liao boundary conditions are also described in detail in [66].
[68] R. W. Ziolkowski, *Optics Express*, vol. 11, pp. 662-681, April 2003.
[69] K. Kunz and R. Luebbers, Eds., *The Finite Difference Time Domain Method for Electromagnetics*, Boca Raton: CRC Press, 1993.
[70] A. Lavrinenko, P. I. Borel, L. H. Frandsen, M. Thorhauge, A. Harpoth, M. Kristensen, and T. Niemi, *Optics Express*, vol. 12, pp. 234-248, January 2004.
[71] R. W. Ziolkowski, "FDTD modeling of photonic nanometer-size power splitters and switches", in *Integrated Photonics Research*, OSA Technical Digest Series, vol. 4, Optical Society of America, 1998, pp. 175.
[72] A. Chutinan and S. Noda, *Appl. Phys. Lett*, vol. 75, pp. 3739-3741, December 1999.
[73] A. Chutinan and S. Noda, *Phys. Rev. B*, vol. 62, pp. 4488-4492, August 2000.
[74] A. Mekis, J. C. Chen, I. Kurland, S. Fan, P. R. Villeneuve, and J. D. Joannopoulos, *Phys. Rev. Lett.*, vol. 77, pp. 3787-3790, October 1996.
[75] R. W. Ziolkowski, "The incorporation of microscopic material models into the FDTD approach for ultrafast optical pulse simulations," in *IEEE Trans. Antennas Propagat.*, vol. 45, pp. 375-391, March 1997.
[76] Marin Soljacic, Chiyan Luo, J. D. Joannopoulos, and S. Fan, *Optics Letters*, vol. 28, pp. 637-639, April 2003.
[77] E. P. Kosmidou and T. D. Tsiboukis, *Opt. Quant. Electr.*, vol. 35, pp. 931-946, August 2003.
[78] C. T. Chan, Q. L. Yu, and K. M. Ho, *Phys. Rev B*, vol. 51, pp. 16635-16642, June 1995.
[79] E. Lidorikis, M. M. Sigalas, E. N. Economou, and C. M. Soukoulis, *Phys. Rev B*, vol. 61, pp. 13458-13464, May 2000.
[80] S. Foteinopoulou, E. N. Economou, and C. M. Soukoulis, *Phys. Rev. Lett.* **90**, 107402-(1-4), March 2003.
[81] X. D. Wang, X.-G. Zhang, Q. Yu, and B. N. Harmon, *Phys. Rev. B*, vol. 47, pp. 4161-4167, February 1993.
[82] N. Stefanou, V. Karathanos, and A. Modinos, *J. Phys.: Condens. Matter*, vol. 4, pp. 7389-7400, September 1992.
[83] Usually the transmitted fields at different detection points after the sample are detected, and an average of the resulting pointing vectors is taken.

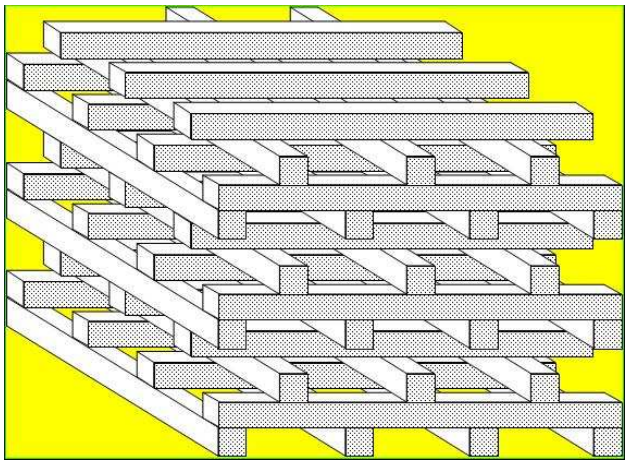

FIG. 1: The layer-by-layer structure, producing a full three-dimensional photonic band gap. The structure is constructed by an orderly stacking of dielectric rods, with a simple one-dimensional pattern of rods in each layer. Although rods of rectangular cross-section are shown here, the rods may be also of circular or elliptical cross sections.

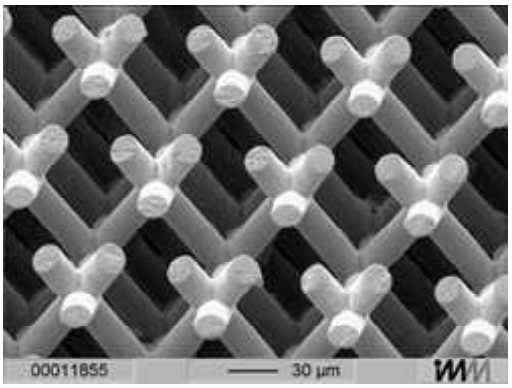


FIG. 2: An "inverse" Yablonovitch' 3-cylinder structure, fabricated by LIGA.

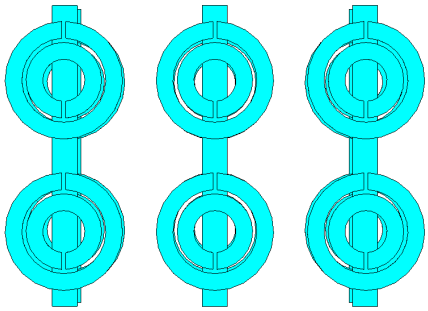

FIG. 3: A schematic of a combination of split ring resonators (SRRs) and continuous wires. Such a combination is the most common way up to now to obtain left-handed materials.

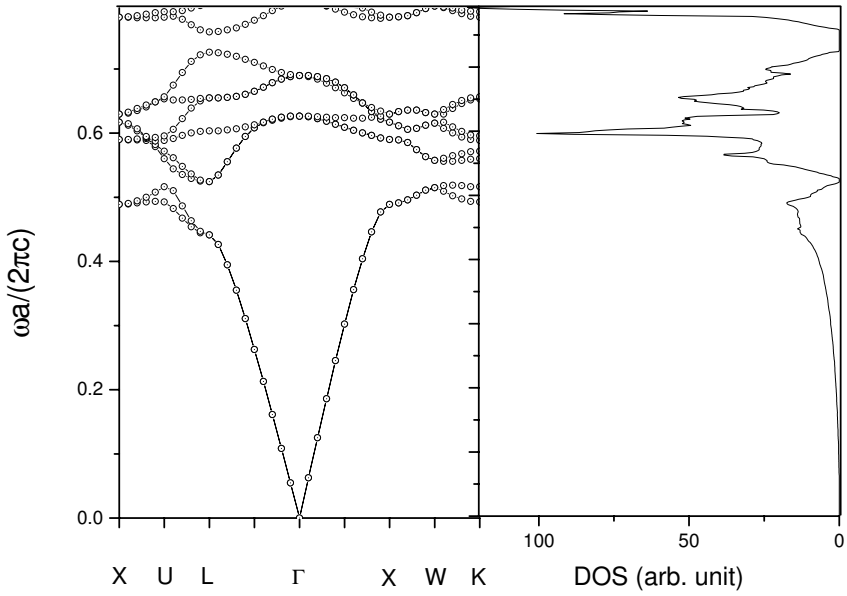


FIG. 4: Band structure (left-plot) and density of states (DOS) calculation (right-plot) for a diamond lattice of dielectric spheres in air. The spheres index of refraction is $n = 3.6$ and their filling ratio 34%. Both the band structure and the DOS are calculated through the plane wave method, employing a very large number of plane waves.

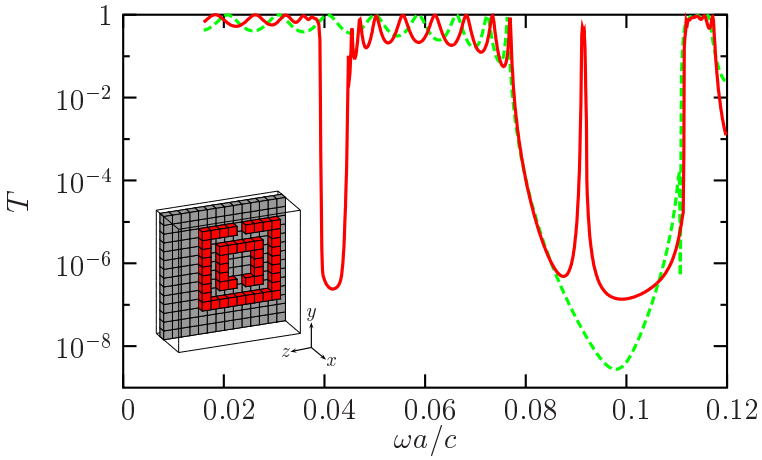


FIG. 5: TMM calculation for the transmission coefficient vs frequency, for a system composed of rectangular split-ring resonators (SRRs) (solid-red line) and for a system of closed-SRRs (SRRs with no gaps) (green-dashed line). The system length along propagation direction is 10 unit cells. The inset shows the geometry of the unit cell (1 SRR attached on a dielectric board). The relative permittivity for the metal is taken to be $\epsilon_m = (-3 + j5.88)10^5$ and for the dielectric board $\epsilon_b = 12.3$. All relative permeabilities are one. The unit cell size is $6a \times 14a \times 14a$. $a$ is the discretization length and $c$ the light velocity in air.

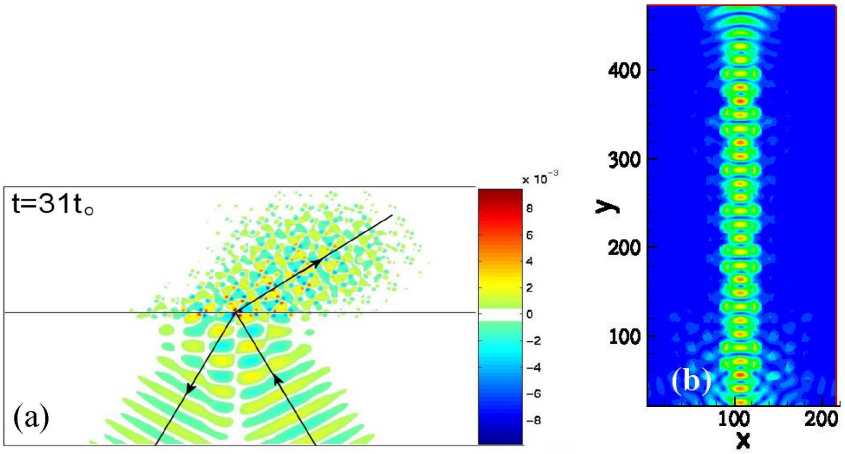


FIG. 6: (a): FDTD picture showing the magnetic field of a TE Gaussian (in space) beam, which undergoes reflection and refraction at the interface between air and a photonic crystal (hexagonal lattice of dielectric rods with $\epsilon = 12.96$ and radius over lattice constant 0.35), for $t = 31t_0$. The frequency of the beam belongs to a "negative" (convex) band of the PC ($a/\lambda = 0.58$, $a$ being the lattice constant, $\lambda$ the free space wavelength), close to the $\Gamma$ inverse-lattice point. $2t_0$ is the time difference between the outer and the inner rays to reach the interface. $t_0 \approx 1.5T$, where $T$ is the period, $2\pi/\omega$, of the wave. (b): The electric field of a TE wave which is guided through a photonic crystal waveguide. The PC waveguide is formed by removing one row of holes, along the $\Gamma$K direction, from a hexagonal 2D photonic crystal (made of cylindrical holes, with radius over lattice constant 0.2463, patterned in a host of $\epsilon = 10.56$). The $a/\lambda$ dimensionless frequency of the guided wave is 0.24. The units in the axes are grid cells of the FDTD discretization scheme.